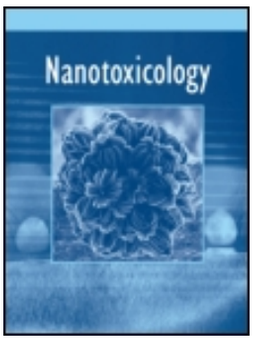

Nanotoxicology

ISSN: 1743-5390 (Print) 1743-5404 (Online) Journal homepage: https://www.tandfonline.com/loi/inan20

The toxicity, transport and uptake of nanoparticles in the *in vitro* BeWo b30 placental cell barrier model used within NanoTEST

Sara Correia Carreira, Laura Walker, Kai Paul & Margaret Saunders

To cite this article: Sara Correia Carreira, Laura Walker, Kai Paul & Margaret Saunders (2015) The toxicity, transport and uptake of nanoparticles in the *in vitro* BeWo b30 placental cell barrier model used within NanoTEST, Nanotoxicology, 9:sup1, 66-78, DOI: 10.3109/17435390.2013.833317

To link to this article: https://doi.org/10.3109/17435390.2013.833317

Accepted author version posted online: 08 Aug 2013.
Published online: 03 Sep 2013.

http://informahealthcare.com/nan
ISSN: 1743-5390 (print), 1743-5404 (electronic)

Nanotoxicology

Nanotoxicology, 2015; 9(S1): 66–78
 DOI: 10.3109/17435390.2013.833317

informa
healthcare

The toxicity, transport and uptake of nanoparticles in the *in vitro* BeWo b30 placental cell barrier model used within NanoTEST

Sara Correia Carreira[1], Laura Walker[2], Kai Paul[3], & Margaret Saunders[4]

[1]*Bristol Centre for Functional Nanomaterials, University of Bristol, Bristol, UK,* [2]*Bristol Heart Institute, School of Clinical Sciences, University of Bristol, Research Floor Level 7, Bristol Royal Infirmary, Bristol, UK,* [3]*Nano Safety Research Group, Heriot-Watt University, School of Life Sciences, Edinburgh, UK, and* [4]*Department of Medical Physics & Bioengineering, BIRCH, Bioengineering, Innovation & Research Hub, St Michael's Hospital, University Hospitals Bristol NHS Foundation Trust, Bristol, UK*

Abstract

Despite the rapid ongoing expansion in the use of nanomaterials, we still know little about their biological interaction and biodistribution within the human body. If medically relevant nanoparticles can cross specific cell barriers they may disseminate through the body beyond the original target and may reach particularly sensitive areas such as the foetus. This study utilised an *in vitro* barrier model of the placenta to explore toxicity, uptake and transport of iron oxide and silica nanoparticles. The findings indicate that these nanoparticles can transfer extensively across the placental barrier model but physico-chemical characteristics such as surface chemistry impact upon both uptake and transport. Iron oxide cytotoxicity was evident at lower doses and shorter exposure compared with silica and may be of clinical relevance. *In vivo* correlation of *in vitro* findings is essential but *in vitro* models may provide worst case-exposure estimates to help reduce the amount of testing required.

Keywords

barrier transport, nanotoxicity, risk assessment, kinetics

History

Received 9 August 2013
Accepted 5 August 2013
Published online 2 September 2013

Introduction

Nanoparticles (NPs) possess unique physico-chemical properties by virtue of their size. Thus NPs have the potential for beneficial use in medicine for improved drug delivery, treatment and imaging due to their ability to operate at the cellular level. However, the same properties also lead to questions about the possible risks associated with such technology (Alexis et al. 2008; Johnston et al. 2013; Medina et al. 2007; Nyström & Fadeel 2012).

Given the vast range of NPs available, it is not feasible to test every nanomaterial in every system. Therefore, there is a need to develop a better understanding of which characteristics are likely to drive a toxic response.

The NanoTEST project, funded as part of the EU Framework 7 Health programme, was designed with the purpose of developing alternative high-throughput testing strategies, using *in vitro* and *in silico* methods, to assess the toxicological profile of NPs relevant to medical diagnostics (Dusinska et al. 2009). A specific part of this project was to evaluate the uptake and transport of a set of medically relevant NPs in a panel of *in vitro* model cellular systems. The aim was to determine whether NPs cross specific cell barriers, allowing further dissemination throughout the body or access to particularly sensitive areas, e.g. foetus during pregnancy. If NPs can reach secondary targets then the potential impact from engineered NPs may need more careful consideration (Iversen et al. 2012).

Correspondence: Margaret Saunders, Department of Medical Physics & Bioengineering, BIRCH, Bioengineering, Innovation & Research Hub, St Michael's Hospital, University Hospitals Bristol NHS Foundation Trust, Southwell St, Bristol BS2 8EG, UK. Tel: +44 117 342 5685. E-mail: M.Saunders@bristol.ac.uk

The placenta plays a key role during pregnancy by transporting nutrients to the developing embryo/foetus that are required to support growth and development (King 1992). Other functions of the placenta include metabolism, immune and endocrine secretion, gas exchange and removal of waste or toxic products. Any interference with the normal function of the placenta may have adverse effects on foetal development and neonatal outcome. Therefore, it is essential to develop an understanding of whether NPs can be taken up and transported across the placental barrier and if they have the potential to cause placental toxicity (Buerki-Thurnherr et al. 2012).

There have been few studies on NP interactions with the placenta or their effects on pregnancy outcome and risks to foetal growth and development. While the ideal approach would be to evaluate the effects of NP exposure in pregnant women, this is not ethically acceptable due to the potential risks. *In vivo* mammalian animal studies have demonstrated placental transfer and foetal uptake of gold, radiolabelled [^{14}C] C60, silver, silica and TiO_2 NP and quantum dots (Chu et al. 2010; Ema et al. 2010; Semmler-Behnke et al. 2008; Sumner et al. 2010; Tang et al. 2009; Yamashita et al. 2011). However, other studies have shown contradictory outcomes with no evidence of NP placental transfer or foetal uptake (Sadauskas et al. 2007) but this may well be due to detection limits. Similarly, contradictory results have been shown using the *ex vivo* perfused human placenta model. Poly(amido amine) (PAMAM) dendrimer conjugates of around 5–6 nm crossed the perfused human placenta in relatively small amounts within 6 h (Menjoge et al. 2011), whereas no PEGylated gold NPs of 10–15 nm were detected on the foetal side after 6-h perfusion (Myllynen et al. 2008). However, fluorescently labelled polystyrene NPs ranging in size from 50 to 240 nm were able to cross the perfused placenta within 3 h (Wick et al. 2010).

Human placental cell-culture models using primary cells or cell lines derived from human placental choriocarcinomas (e.g. BeWo, JEG-3 or Jar) provide an *in vitro* alternative enabling quantitative assessment of NP transfer (Saunders 2009). An *in vitro* study of gold NPs coated with polyethylene glycol demonstrated the uptake and retention of 10 nm diameter NP for up to 48 h after exposure of BeWo cells (ATCC clone) grown on plastic Petri dishes as analysed by transmission electron microscope (TEM) (Myllynen et al. 2008). More recently, the BeWo b30 Transwell model was optimised for use with fluorescent polystyrene latex Fluoresbrite NPs (Cartwright et al. 2012). It was shown that transport of the NPs across an intact BeWo b30 monolayer was size dependent with smaller 50–nm-diameter particles being transferred at a higher rate compared with larger 100-nm particles, up to 24 h after addition of NPs.

Superparamagnetic iron oxide NPs are being used as contrast agents for magnetic resonance imaging (MRI) (Halamoda Kenzaoui et al. 2012a; Mahmoudi et al. 2011; Qiao et al. 2009; Rümenapp et al. 2012) and are in development with different coatings for imaging, as drug-delivery vehicles and for cell labelling and tracking (Andreas et al. 2012; Gambarota et al. 2010; Halamoda Kenzaoui et al. 2012b; Kumagai et al. 2010; Rosen et al. 2012; Sekhon & Kamboj 2010; Wahajuddin 2012; Yigit et al. 2012; Zou et al. 2010). However, given the current lack of knowledge about the effects of such agents during pregnancy, their clinical use is subject to risk/benefit analysis on a case-by-case basis and it is recommended that their use during the first trimester in particular should be avoided where possible (MHRA 2007). Therefore, this may lead to a pregnant woman being denied the most effective treatment or diagnostic test at a crucial time.

Silica NPs are being manufactured for biomedical purposes which include medical imaging and drug delivery but concerns about possible toxicity need to be addressed before they can be widely implemented (Fadeel & Garcia-Bennett 2010). Mesoporous silica NPs are of particular interest for biomedical applications due to their stable structure, ease of modification due to accessible internal and external structures and good biocompatibility. Key applications at the preclinical stage include nucleotide and drug delivery, optical imaging and MRI (Choi et al. 2012; Tang et al. 2012; Yang et al. 2012). Fluorescent silica NPs are also being developed for the purposes of sentinel lymph node mapping, real-time imaging of tumour metastasis and cell tracking in mice as well as fluorescent biosensing (Choi et al. 2007; Zhao et al. 2007; Zhong 2009).

This study evaluated NP toxicity and cell barrier transport, using the BeWo b30 placental barrier model. Fully characterised iron oxide NPs with different surface chemistry and silica NPs of different sizes at a range of different NP concentrations were used as medically relevant test NPs.

Methods

Reagents and chemicals

Cell-culture medium and supplements, trypsin-EDTA, sodium fluorescein solution (Na-Flu), phosphate buffered saline, hydrochloric acid (HCl), potassium hexacyanoferrate (II), paraformaldehyde and Triton X-100 were purchased from Sigma-Aldrich (Gillingham, UK). Primary polyclonal antibody for tight junction staining was mouse anti-human ZO-1 from Life Technologies Ltd (Paisley, UK). The secondary antibody was Alexa Fluor® 488 donkey anti-mouse from Invitrogen (Life Technologies Ltd, Paisley, UK). Vectashield mounting medium with DAPI was obtained from Vector Laboratories Ltd (Peterborough, UK).

Nanoparticles

Nanomagnetite uncoated iron oxide (U-Fe_3O_4) and Na-oleate-coated (OC-Fe_3O_4) NPs were purchased from Plasmachem (Berlin, Germany) with a nominal diameter of 8 nm. They were supplied in water at 28 or 260 mg/ml, respectively, and stored at 4 °C. Fluorescent rhodamine-labelled silica 25 nm (Fl-25 SiO_2) and 50 nm (Fl-50 SiO_2) NPs were purchased from Corpuscular (Cold Spring, New York, USA) as stock suspensions at 25 mg/ml in water and were stored at 4 °C. A summary of the NP characterisation is shown in Table I with full methods and results described in Guadagnini et al. (2015).

Cell models and culture conditions

The placental choriocarcinoma cell line BeWo b30 was used for the placental barrier model and obtained from Prof Harry McArdle (Rowett Research Institute, Aberdeen) with permission from Dr. Alan Schwartz (Washington University, St. Louis, MO, USA). Cells were cultured in complete medium supplemented with 10% fetal bovine serum as described previously (Cartwright et al. 2012) with or without phenol red. The BeWo b30 cell lineage has been authenticated by the European Cell and Culture Collection (Jones et al. 2006). At confluence, cells were subcultured using a 0.4% trypsin–EDTA solution.

Toxicity testing

BeWo b30 cells were seeded at 2.5×10^5 cells/ml and grown until approximately 70% confluent. For toxicity testing, cells were treated for 4, 24 or 48 h, with NPs at the following concentrations: 75, 15, 3, 0.6 and 0.12 μg/cm^2.

Cytotoxicity was evaluated by measuring lactase dehydrogenase (LDH) in the cell-culture medium of exposed and untreated cells with the CytoTox 96® non-radioactive cytotoxicity assay kit from Promega (Southampton, UK). The assay was conducted as per the manufacturer's instructions.

Table I. Summary of physico-chemical properties of Fe_3O_4 and Fl-SiO_2 NPs characterised in DMEM-F12-HAM medium.

	OC-Fe_3O_4	U-Fe_3O_4	Fl-25 SiO_2	Fl-50 SiO_2
Crystal structure	Spinel octahedral		amorphous	
Primary size (nm)	9×7[1]	10×7[1]	15–30[2]	25–50[2]
Crystallite size distribution by TEM (nm)	5–12	5–13	15–30	25–50
Surface chemistry	Na-oleate micelle coating	Uncoated	Uncoated	Uncoated
Zeta potential in milliQ water at pH 7 (mV)	–31.9	–2.8	–20	–22
Average size in original suspension by DLS (nm)	–[3]	–[3]	26	38
Average hydrodynamic diameter in medium by DLS	Bimodal distribution: 31, 132 nm	Large agglomerates: 1–50 μm	26 nm	40 nm
Size stability in medium by DLS	~3 days	<5 min	<20 h	<20 h

[1]Oblong shape; [2]By TEM; [3]Too high concentration for DLS measurement.

To assess cellular metabolism after NP exposure, WST-1 reagent was used (Roche Diagnostics Ltd, Burgess Hill, UK). After the respective exposure times, 10 µl of WST-1 reagent was added to each well and the plate was incubated for 3.5 h at 37 ºC. Following incubation, absorbance was measured at 450 nm using a FluoSTAR OPTIMA fluorescence microplate reader.

Cytokine (IL-6) levels in cell-culture supernatants were measured using the IL-6 ELISA assay (Invitrogen, UK) as outlined by the manufacturer. Total protein concentration was determined using the bicinchoninic acid assay (Thermo Fisher Scientific, Loughborough, UK) to allow for subsequent correction of variation in cell number.

For the LDH and WST-1 assay, optical density (OD) values of wells containing treated cells were expressed as a percentage of the OD values of the untreated control: % of control = OD treated/OD untreated × 100. For the ELISA, IL-6 concentration in cell-culture supernatants was determined from the standard curve and expressed as protein-corrected values (pg/ml/mg of total protein).

The morphology of BeWo b30 cells grown on poly-L-lysine-coated glass cover slips exposed to the highest and lowest concentration of NP for 48 h was examined using light microscopy.

Transport and uptake of NPs

Model development

Transwell® plates (Costar) with polyester (PE) and polycarbonate (PC) membranes of 3 µm pore size were obtained from Appleton Woods Ltd (Birmingham, UK). BeWo b30 were seeded at 10^5 cells/cm^2 on PE and PC inserts pre-soaked in medium for 45 min. Medium was changed on days 3, 4 and 5 post-seeding (ps). Development of the monolayer on both membrane types was monitored using Na-Flu transport on days 2, 3, 4 and 5.

BeWo b30 cells grown on inserts were examined in the light microscope to visualise monolayer formation. Cell layers were fixed with 4% glutaraldehyde, membrane inserts cut out from the holder and embedded in a resin block. One-micrometre sections were cut from the block and stained with toluidine blue. To examine the presence of tight junctions in the monolayer, antibody staining was performed on BeWo b30 grown on PE inserts on day 4 ps. Cells on inserts were fixed in 2% paraformaldehyde and permeabilised with 0.5% Triton X-100. Cells were incubated with primary antibody against ZO-1 and washed before incubation with the secondary antibody. Membrane inserts were cut out from the holder and mounted on slides using VectaShield with DAPI. The staining was observed using a Leica SP5 confocal attached to a Leica DMI 6000 inverted microscope and a 63× (1.4 numerical aperture [NA]) oil-immersion objective.

NP transport experiments

BeWo b30 cells were seeded at 10^5 cells/cm^2 on Transwell® PE inserts of 3 µm pore size. Medium was changed on day 3 ps and experiments were conducted on day 4 ps at 37 °C in a humidified 5% CO_2 atmosphere. Transport of each particle type was examined across three inserts with cells and three blank inserts (i.e. without cells).

The transport time course was evaluated in Transwell® chambers for up to 6 h (Fl-SiO_2 NP at 25 or 50 µg/ml) or up to 24 h (Fe_3O_4 NP at 50 or 100 µg/ml) comparing transport across the permeable PE insert in the presence or absence (blanks) of a confluent BeWo cell monolayer. A shorter time course was chosen for Fl-SiO_2, because we had observed significant loss of fluorescence intensity after 6 h.

For each NP suspension, 0.5 ml was added to the apical chamber of the Transwell® system, and 1.5 ml of medium was added to the basal chamber. At the appropriate time points, 50-µl samples were harvested from the basal chambers into 96-well plates and replaced with fresh medium to compensate for the loss of volume. To estimate association and uptake of Fl-SiO_2 and Fe_3O_4 NP with the BeWo b30 cells after the transport experiments, cells were washed, harvested and permeabilised with 0.3% Triton X-100 for 1 h. The amount of iron was assessed by Prussian Blue reaction, and localisation of Fe_3O_4 NP was visualised using an FEI Tecnai12 Biotwin transmission electron microscope equipped with a bottom-mount 4*4k Eagle CCD camera after preparation for TEM imaging according to Lahtinen et al (2003). For the Fl-SiO_2 NPs, samples were analysed by measurement on a microplate reader at 545 nm excitation and 590 nm emission. Association of Fl-SiO_2 NPs was also assessed qualitatively by visualisation of the inserts by confocal microscopy using a Leica SP5 confocal attached to a Leica DMI 6000 inverted microscope and a 40× (1.4 NA) oil-immersion objective.

For the samples taken in the transport experiments at each time point (t_n), the cumulative amount (Q_n) transported to the basal chamber was determined and corrected for the mass removed during previous sampling:

$$Q_n = C_n \cdot V_b + \sum_{j=1}^{n-1} Vs \cdot Cj$$

where C_n is the concentration of NPs in the sample measured at t_n, V_b is the volume in the basal chamber (1.5 ml), V_s is the sampling volume (0.05 ml) and the summation term represents the correction for the cumulative mass removed by sampling previously (from $t = t_1$ until $t = tn$-1). The cumulative amounts transported were plotted over time and the linear appearance rate (slope = $\Delta Q/\Delta t$) of NPs in the basal chamber determined. The apparent permeability coefficient P_{app} across blank inserts and inserts with cells was estimated for each NP and starting concentration according to the following equation (Gao et al. 2000):

$$P_{app} = \frac{\Delta Q / \Delta t}{A \cdot C0}$$

where $\Delta Q/\Delta t$ is the linear appearance rate of the NP in the basal chamber (µg/sec), A is the surface area of the insert membrane (1.12 cm^2) and C_0 is the initial concentration of the compound in the apical chamber (mmol/cm^3). The permeability coefficient (P_e) across BeWo cells was calculated using the following equation (Liu et al. 1997):

$$\frac{1}{P_e} = \frac{1}{P_{app}} - \frac{1}{BlankP_{app}}$$

where P_{app} is the mean apparent permeability coefficient for the insert membranes in the presence of BeWo cell monolayers, and $BlankP_{app}$ is the mean apparent permeability coefficient for the blank insert membranes.

Lastly, barrier toxicity of the NPs was evaluated using the sodium fluorescein (Na-Flu) permeability assay. Na-Flu transport was assessed across unexposed and NP-exposed BeWo b30 barriers by adding a 5-µM solution of Na-Flu to the apical chamber and sampling from the basal chamber over 3–4 h. Furthermore, exposed barriers were stained with ZO-1 (as described above) to examine whether tight junctions stayed intact.

Statistical analysis

Data are presented as mean ± SD of three independent experiments. Statistical analysis was performed using SPSS v18

for Windows. Results from the LDH assay were analysed by one-way analysis of variance (ANOVA) with *post hoc* contrast analysis. WST-1 and ELISA data were analysed by ANOVA followed by Games Howell multiple comparison procedure. For the transport experiments, results were analysed using one-way ANOVA to compare dye transport across untreated cell layers and cell layers exposed to Fe_3O_4 and Fl-SiO_2 NP. Effects of particle characteristics (size or coating) and initial particle concentration in the apical chamber on P_e and association with cells were explored using two-way ANOVA. Statistical probability of $p < 0.05$ was considered significant.

Results

Toxicity

LDH

The LDH assay gives an indication of cytotoxicity by assessing the extent of LDH release into the culture medium as a result of membrane leakage. To determine whether LDH release was dose- and time-dependent, BeWo b30 cells were exposed to U-Fe_3O_4 or OC-Fe_3O_4 NPs (see Figure 1A) or Fl-25 or Fl-50 SiO_2 NPs (see Figure 1B) for 4, 24 or 48 h with $p < 0.05$ considered significant. After 4-h exposure, LDH levels were significantly above the untreated control for cells exposed to the highest concentration of either type of Fe_3O_4 NP. After 24-h exposure, significant LDH release was observed for cells exposed to all concentrations of U-Fe_3O_4 except 3 μg/cm^2 and the lowest and highest concentrations of OC-Fe_3O_4 NPs. After 48-h exposure, LDH levels were elevated in media taken from cells treated with 75 and 15 μg/cm^2 of U-Fe_3O_4 and 3–75 μg/cm^2 of OC-Fe_3O_4 NPs. Notably, LDH levels in culture supernatants of cells treated with the highest concentration of OC-Fe_3O_4 increased substantially compared with the lower concentrations and the 1 mM H_2O_2 positive control. A significant time-dependent increase was seen at the higher concentrations (15 and 75 μg/cm^2) for U-Fe_3O_4 but not for OC-Fe_3O_4 NP exposure. In contrast, no significant LDH release was observed following exposure to Fl-25 or Fl-50 SiO_2 NPs at any concentration after 4 h (Figure 1B). After 24- and 48-h

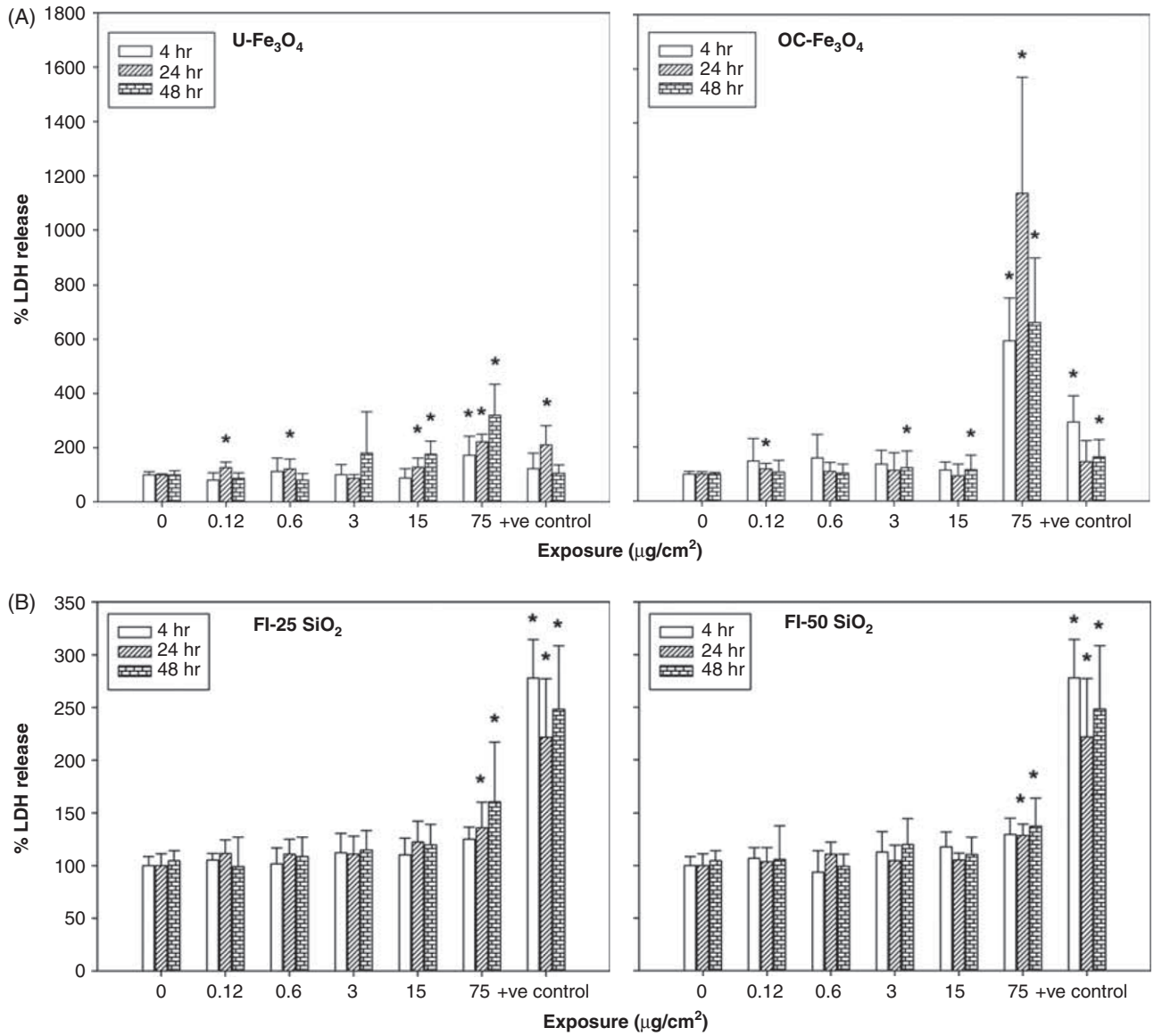

Figure 1. (A) LDH release from BeWo b30 cells exposed to U- or OC-Fe_3O_4 NPs for 4, 24 and 48 h. Values represent average % of untreated control ± SD of three separate experiments (total of $n = 12$ per treatment). To induce cell death (positive control), 1 mM H_2O_2 was used. *Denotes statistically significant difference from the unexposed control ($p < 0.05$). (B) LDH release from BeWo b30 cells exposed to 25 and 50 nm Fl-SiO_2 NPs for 4, 24 and 48 h. Values represent average % of untreated control ± SD of three separate experiments (total of $n = 12$ per treatment). To induce cell death (positive control), 0.1% DMSO was used. *Denotes statistically significant difference from the unexposed control ($p < 0.05$).

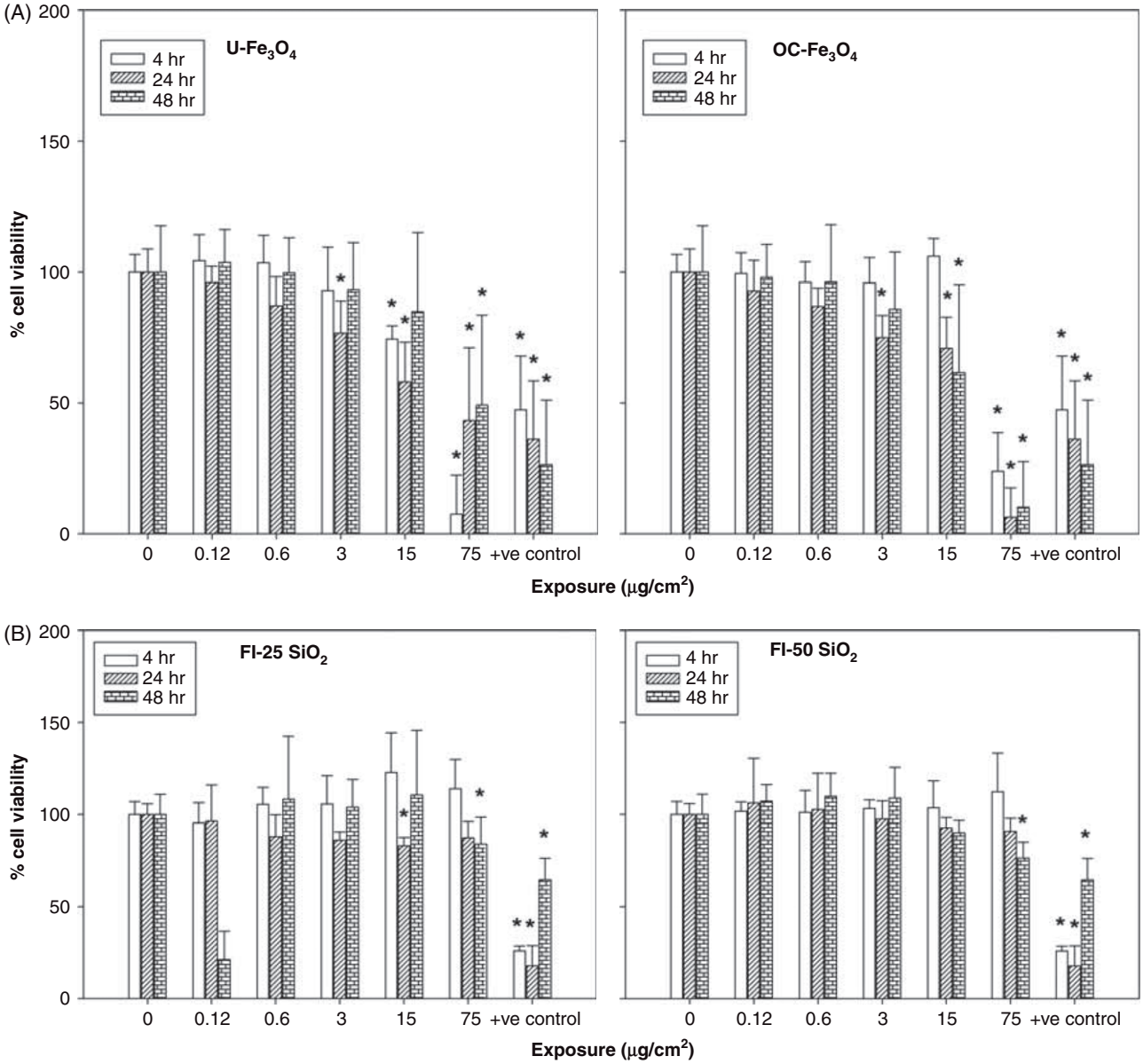

Figure 2. (A) Cell viability of BeWo b30 cells exposed to U-Fe_3O_4 or OC-Fe_3O_4 NPs for 4, 24 and 48 h as measured by WST-1 assay. Values represent average % of untreated control ± SD of three separate experiments (total of $n = 12$ per treatment). To induce cell death (positive control), 0.1% DMSO was used. *Denotes statistically significant difference from the control ($p < 0.05$). (B) Cell viability of BeWo b30 cells exposed to Fl-25 and Fl-50 SiO_2 NPs for 4, 24 and 48 h as measured by WST-1 assay. Values represent average % of untreated control ± SD of three separate experiments (total of $n = 12$ per treatment). To induce cell death (positive control), 0.1% DMSO was used. *Denotes statistically significant difference from the control ($p < 0.05$).

exposure, significant LDH release was observed only for the highest concentration (75 μg/cm^2) of Fl-25 or Fl-50 SiO_2 NPs.

WST-1

This assay gives an indication of cell viability by measuring cellular WST-1 metabolism. To determine whether cell viability was affected in a dose- and time-dependent manner, BeWo b30 cells were exposed to U- or OC-Fe_3O_4 NPs (see Figure 2A) or Fl-25 or Fl-50 SiO_2 NPs (see Figure 2B) as described above. Cell viability was significantly reduced in cells treated with 15 and 75 μg/cm^2 of U-Fe_3O_4 and 75 μg/cm^2 of OC-Fe_3O_4 for 4 h. After 24-h exposure, concentrations of 3, 15 and 75 μg/cm^2 of both Fe_3O_4 NP types resulted in significantly reduced cell viability. Notably, cell viability was more drastically reduced in cells exposed to the highest concentration of OC-Fe_3O_4 compared to cells exposed to the highest concentration of U-Fe_3O_4. Finally, cell viability decreased significantly compared to unexposed cells after 48-h exposure to both 15 and 75 μg/cm^2 of OC-Fe_3O_4. However, for U-Fe_3O_4, cell viability was only affected after 48-h exposure to 75 μg/cm^2.

For the Fl-25 SiO_2 NPs, a significant decrease in cell viability was observed 4-h post-exposure to 15 μg/cm^2. After 24-h exposure, there was no effect on cell viability for either Fl-SiO_2 particle size. There was a reduction in cell viability 48-h post-exposure to 75 μg/cm^2 for both sizes of Fl-SiO_2 NP.

IL-6

IL-6 is an inflammatory cytokine produced by the placenta. The release of IL-6 from BeWo b30 cells after 4, 24- and 48-h exposure to U-Fe_3O_4 and OC-Fe_3O_4 (Figure 3A) and Fl-25 and Fl-50 SiO_2 NPs (Figure 3B) across the aforementioned concentration range was determined using an ELISA assay. Generally,

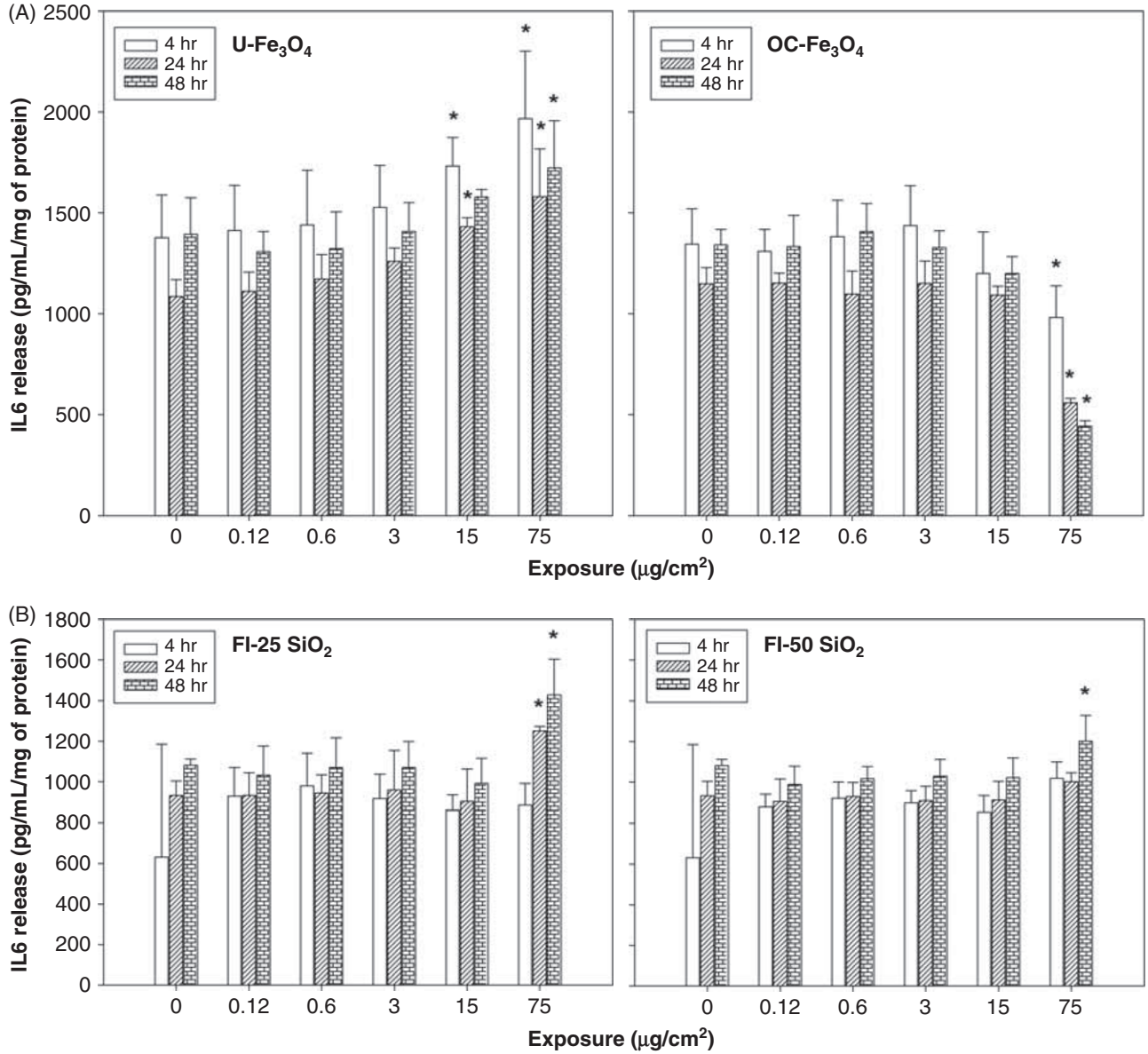

Figure 3. (A) IL-6 release from BeWo b30 cells exposed to U-Fe_3O_4 NP and OC- Fe_3O_4 NPs for 4, 24 and 48 h as determined by ELISA. Values represent average % of untreated control ± SD of three separate experiments (total of $n = 6$ per treatment). *Denotes statistically significant difference from the unexposed control ($p < 0.05$). (B) IL-6 release from BeWo b30 cells exposed to 25 and 50 nm Fl-SiO_2 NPs for 4, 24 and 48 h as determined by ELISA. Values represent average % of untreated control ± SD of three separate experiments (total of $n = 6$ per treatment). *Denotes statistically significant difference from the control ($p < 0.05$).

concentrations up to 3 μg/cm^2 of either particle type did not induce a significant change of IL-6 concentration in the medium at any exposure time. Exposure of BeWo b30 cells to 15 and 75 μg/cm^2 of U-Fe_3O_4 resulted in a significant increase in IL-6 released at 4- and 24-h post-exposure, as compared to untreated controls. After 48 h, cells exposed to 75 μg/cm^2 U-Fe_3O_4 released significantly more IL-6 than untreated cells. Exposure to OC-Fe_3O_4 resulted in a very different pattern: IL-6 concentration in media from cells exposed to 75 μg/cm^2 was significantly reduced compared to the untreated cells after each exposure time point. The IL-6 concentration in the cell media was not significantly different compared with that from the unexposed cells for any of the time points following exposure to 0.12–15 μg/cm^2 of OC-Fe_3O_4 NPs.

IL-6 levels were similar in media from both SiO_2 treated and untreated cells after 4-h exposure. Twenty-four-hour exposure to the highest concentration of Fl-25 SiO_2 NPs resulted in significantly elevated IL-6 levels compared to untreated cells, but this was not the case for Fl-50 SiO_2 NPs. Finally, 48-h exposure to the highest concentration of both sizes of SiO_2 NPs resulted in higher IL-6 concentrations compared to the untreated control. All other treatments did not result in any significant change in IL-6 concentration in cell-culture supernatants as compared with the unexposed controls.

Morphology of BeWo b30 after long-term exposure

To examine the morphology of cells exposed to the highest and lowest concentration of all four NPs for 48 h, light microscopy was employed. No significant changes in morphology were observed when cells were exposed to the lowest concentration of either NP (Figure 4). Exposure to the highest concentration of Fl-SiO_2 and U-Fe_3O_4 leads to a decrease in the number of attached cells, their morphology still resembling that of unexposed cells. However, exposure to high concentrations of OC-Fe_3O_4 led to a significant decrease in cell number and morphology was markedly changed. Cells appeared disconnected from each other, and smaller compared to unexposed cells (Figure 4).

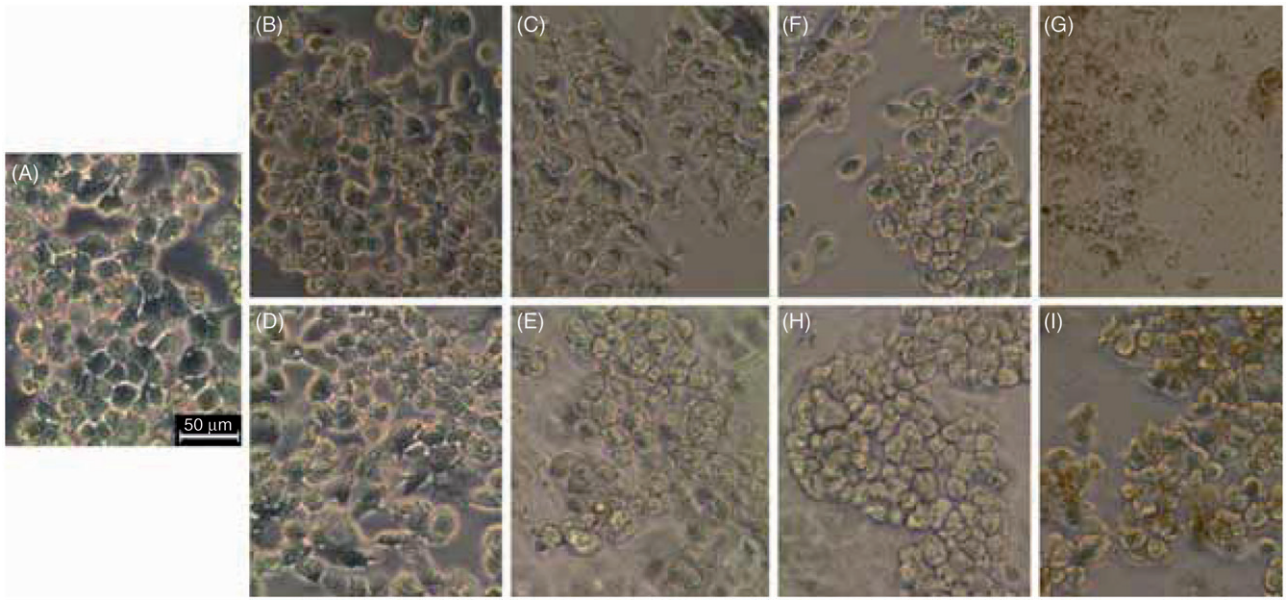

Figure 4. Light microscopic images of BeWo b30 grown on poly-L-lysine-coated glass cover slips. Unexposed cells shown in A. Cells exposed to low (0.12 µg/cm^2) and high (75 µg/cm^2) concentrations of NPs for 48 h shown in B–I. Scale bar shown in A is representative for images B–I, too. B–E: Cells exposed to low (B) and high (C) concentrations of 25 nm Fl-SiO_2, and low (D) and high (E) concentrations of 50 nm Fl-SiO_2. F–I: Cells exposed to low (F) and high (G) concentrations of OC-Fe_3O_4, and low (H) and high (I) concentrations of U-Fe_3O_4.

Figure 5. Imaging of BeWo b30 grown on PE 3 µm pore inserts on day 4 ps. Medium changed on day 3 ps. Left: light microscopic image showing cells stained with toluidine blue. Right: tight junctions (green) visualised with ZO-1 immunostaining in confocal microscope; nuclei stained with DAPI appear blue; white scale bar represents 48 µm.

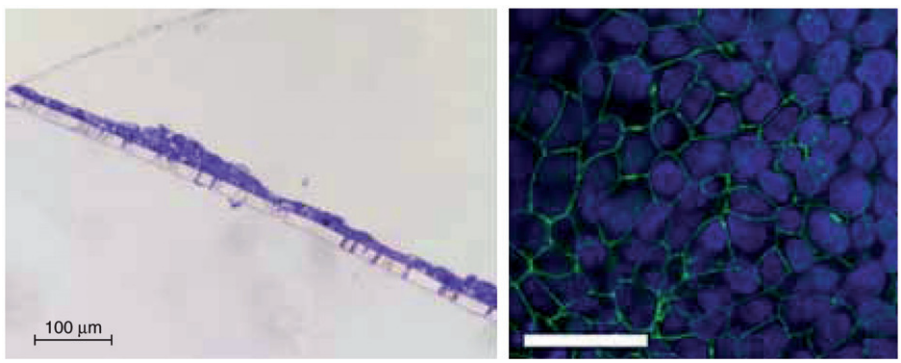

Transport and uptake

Whilst membrane pore size is not an issue of concern when evaluating the transport of solutions across the cell barrier, we chose to use inserts with a larger pore size (3 µm) in this study of NP suspensions to avoid potential clogging of smaller pore sizes by agglomerated NPs. PE inserts appeared more suitable for growing BeWo b30 cells (data not shown), and because little particle adherence was observed after 24 h for either PE or PC inserts, we decided to use PE instead of PC inserts for the transport studies. BeWo b30 formed a confluent monolayer with fully developed tight junctions on day 4 ps as confirmed by light microscopy and ZO-1 staining (Figure 5).

Transport and uptake of NPs

Fe_3O_4 NPs

Particle coating of Fe_3O_4 NPs greatly influenced both the transport and association of the NPs with cells. Coating with Na-oleate resulted in extensive transport of Fe_3O_4 across the cells (Figure 6) and very little association with cells (Table II) but NP concentration (50 or 100 µg/ml) made no significant difference to the extent of transport across the cell barrier. However, more OC-Fe_3O_4 NPs were detected in the basal chamber in the absence of BeWo cells when a higher dose was used (Figure 6).

U-Fe_3O_4 NPs were shown to be unstable in cell-culture media (Table I) and very quickly agglomerated and precipitated onto the permeable insert. Evaluation of samples from the basal chamber demonstrated that there was no significant difference between inserts with and without BeWo cell layers. Visually, the pores appeared to be blocked by the NPs. Considerable amounts of Fe_3O_4 were detected in association with the cells after 24-h exposure to 100 µg/ml NPs in the Transwell: 7.96 ± 1.92 µg for U-Fe_3O_4 as compared to 0.32 ± 0.55 µg for OC-Fe_3O_4 NPs (see also Figure 7).

Fl-SiO_2 NPs

There was no significant effect of particle size or initial concentration on transport or association of Fl-SiO_2 NPs with the cells (Figures 6 and 8, Table II). Similar amounts of both Fl-SiO_2 NP sizes transferred across the BeWo cell layer at both initial concentrations (Figure 6). However, more Fl-SiO_2 NPs were detected in the basal chamber in the absence of BeWo cells when a higher dose was used. Regardless of particle size or initial concentration, similar amounts of Fl-SiO_2 associated with the cells.

Comparison of NP transport

A comparison of OC-Fe_3O_4, Fl-25 and Fl-50 SiO_2 transport using an initial concentration of 50 µg/ml over 6 h demonstrated similar

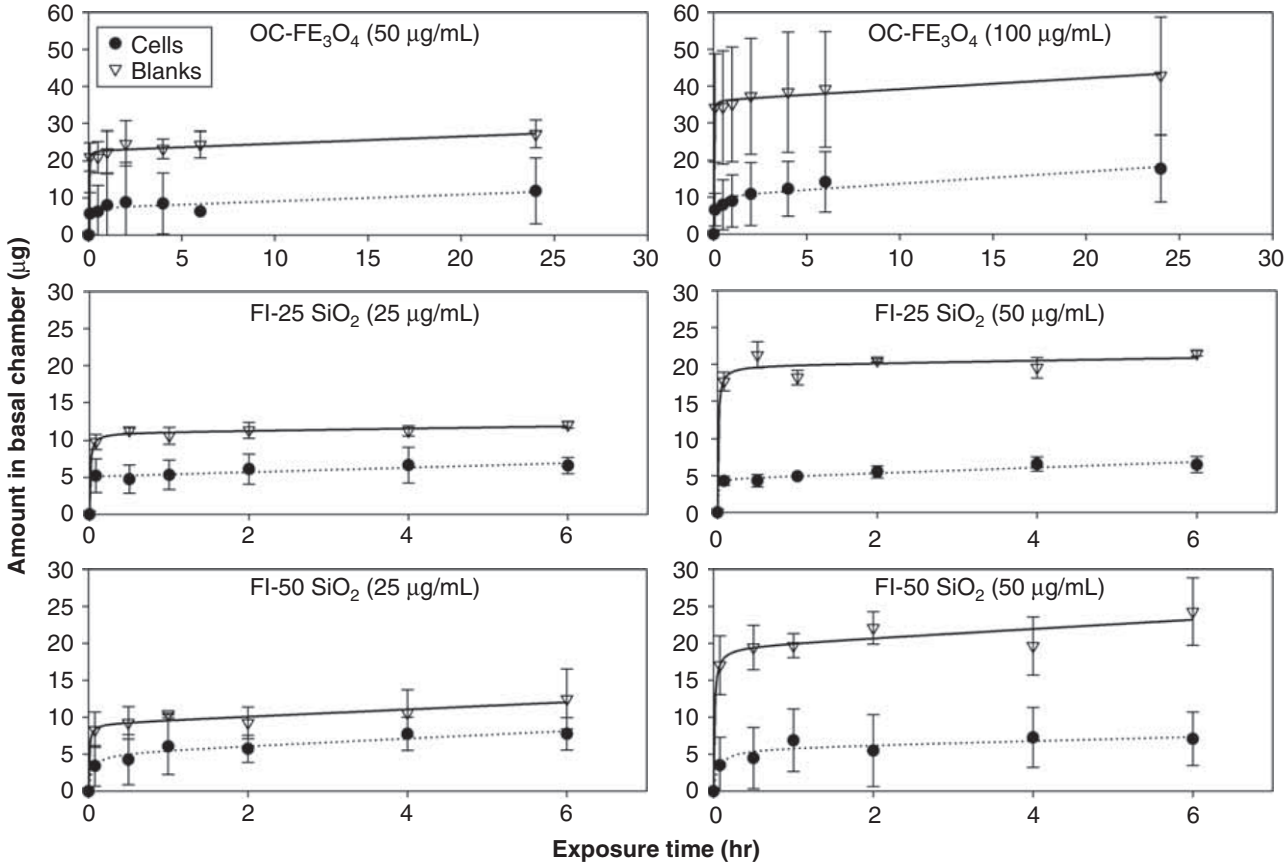

Figure 6. Transport of NPs across the BeWo b30 barrier. The appearance of OC-Fe_3O_4 NPs in the basal chamber was determined over 24 h, and appearance of 25 and 50 nm Fl-SiO_2 in the basal chamber over 6 h. A total of three Transwells® were sampled per time point for each experiment, and sampled volume was replaced with medium. Values were corrected for this sampling and replacement. Initial concentrations added to the apical chamber at $t = 0$ h were 50 or 100 μg/ml for OC-Fe_3O_4 NPs, and 25 or 50 μg/ml for Fl-SiO_2 NPs. Results are shown for transport in the presence (dotted line, circles) and absence (continuous line, triangles) of BeWo cells. Values expressed as mean ± SD from three separate experiments.

Table II. Permeability coefficients (P_e) across BeWo b30 cell barriers, percentage transport and association of OC-Fe_3O_4, Fl-25 and Fl-50 SiO_2 NPs.

NP	P_e (cm/sec)	% Transported across blanks	% Transported across cells	% Association with cells
OC-Fe_3O_4	0.017 ± 0.002	84.0 ± 6.2	24.1 ± 3.0	1.2 ± 1.7*
Fl-25 SiO_2	0.018 ± 0.007	81.4 ± 3.6	26.2 ± 0.8	3.3 ± 2.2
Fl-50 SiO_2	0.017 ± 0.009	87.8 ± 15.0	29.0 ± 8.9	3.7 ± 3.1

Measurements were made after 6-h exposure to NPs of BeWo b30 cells grown on PE inserts (initial concentration in the apical chamber 50 μg/ml). Percentages were calculated with respect to the amount of NP added to the apical chamber at the beginning of the time course. Amounts of iron in cells and inserts were measured with Prussian Blue reaction. Amounts of Fl-SiO_2 in cells were determined by measuring fluorescence intensity. Values expressed as mean ± SD from three separate experiments (three replicates in each). *Represents significant difference ($p < 0.05$) between OC-Fe_3O_4 and Fl-25 and Fl-50 SiO_2 association with cells.

transfer of each NP type across the BeWo b30 cell barrier to the basal chamber (Table II). Permeability coefficients were similar for all three NP types but association of NP with cells was higher for Fl-SiO_2 compared with OC-Fe_3O_4 NPs. Furthermore, NaFlu transport across exposed and unexposed BeWo b30 was similar (data not shown) and ZO-1 staining of exposed cells on the inserts revealed that tight junctions were still present (Figures 8 and 9).

Imaging of exposed cell monolayers

Inserts from the transport experiments were processed for imaging to investigate cellular association and compartmentalisation of Fe_3O_4 and Fl-SiO_2 NP. U-Fe_3O_4 and OC-Fe_3O_4 NPs could be clearly observed using TEM (Figure 7). Whilst OC-Fe_3O_4 NPs were not visible externally, they can be clearly visualised as dense patches within the cell and appear to be localised within intracellular vesicles (Figure 7B). In contrast, U-Fe_3O_4 NPs are seen as precipitated clumps external to the cell membrane (Figure 7C). These clumps of NPs also show endocytic activity, appearing as electron-dense patches. In Figure 7D, the NP clumps appear contained within what may be a clathrin pit, as evidenced by the electron-dense material coating the edge of the pit at the bottom of the image.

To visualise Fl-SiO_2 on BeWo b30-exposed cell layers, we utilised confocal imaging (Figure 8). The NPs were shown to be present in the cell preparations after processing and the number of particles can be seen to increase slightly with dose (B vs A and D vs C). From the sequential Z-stack scans it could be observed that whilst most Fl-SiO_2 NPs were localised on the surface of the cells, some NPs could be seen inside the cells.

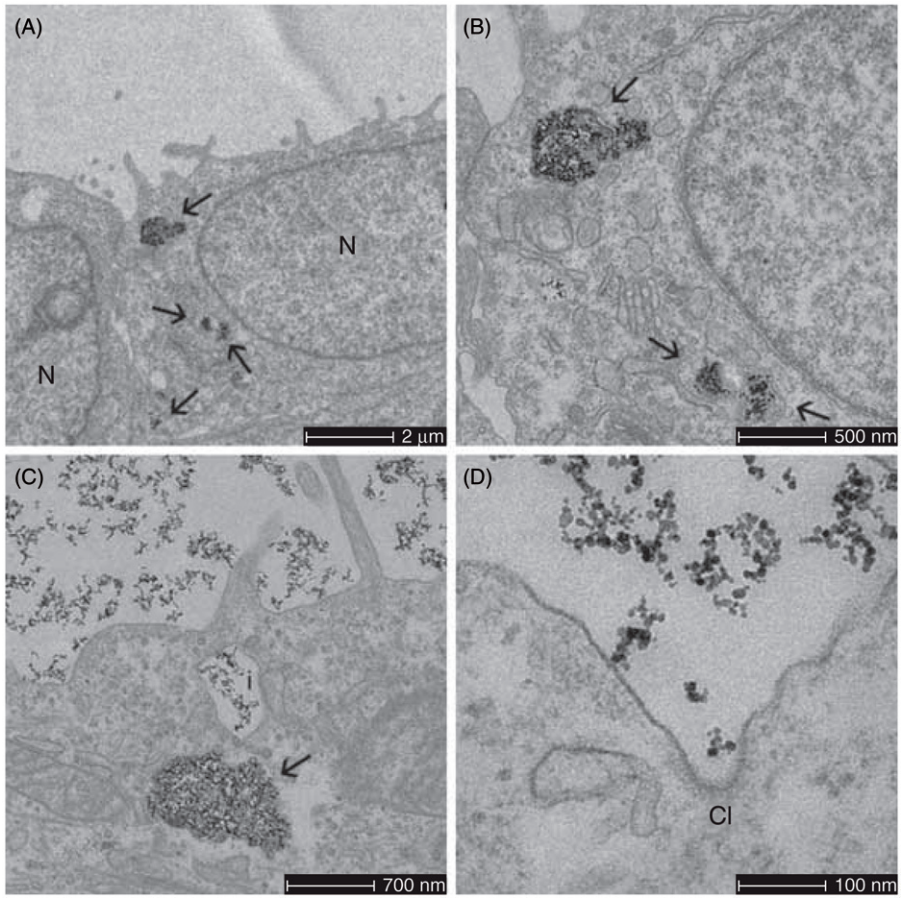

Figure 7. TEM imaging of BeWo b30 cells after exposure to Fe_3O_4 NPs. BeWo b30 cells grown on PE membranes with 3 µm pore size were imaged after exposure to OC-Fe_3O_4 (A and B) or U-Fe_3O_4 (C and D) NPs for 24 h. N – nucleus; Cl – clathrin pit; i – intercellular space; arrows indicate presence of Fe_3O_4 NP.

Discussion

As the use of nanotechnology continues to expand, it is critical that we understand the health risks associated with NPs and establish the parameters required for their safe use. Due to the complexities associated with nanoscale materials, we cannot use a ''one size fits all'' approach. At the same time, we do not have the resources to evaluate every single particle type. Therefore, it is essential to determine which NP properties induce which effects in a panel of NPs. This is the essence of the NanoTEST project and as part of this study we have evaluated the suitability of the BeWo b30 placental barrier model for determining NP toxicity and transport with regard to NP size and surface chemistry.

The toxicity of Fe_3O_4 and Fl-SiO_2 NPs was assessed using a range of assays. The use of several different approaches is important as NPs have been shown to induce toxicity using a variety of mechanisms including cell membrane damage, oxidative stress and DNA damage (Brunner et al. 2006; Johnston et al. 2010; Naqvi et al. 2010; Unfried et al. 2007).

Results from our toxicity studies indicate that the surface chemistry of Fe_3O_4 NPs with similar core size plays an important role in terms of toxicity outcome. Oleic acid is a commonly used surfactant which stabilises Fe_3O_4 NPs with a strong chemical bond formed between the carboxylic acid and Fe_3O_4 NPs and reduces interactions between the NPs (Zhang et al. 2006). Reduction in cell viability and increased membrane damage were more pronounced for OC-Fe_3O_4 NP compared to U-Fe_3O_4 NP at the highest exposure dose. IL-6 release was markedly different when BeWo b30 cells were exposed to OC-Fe_3O_4 compared to U-Fe_3O_4. Exposure to U-Fe_3O_4 NPs resulted in an increase of IL-6 levels, whereas exposure to OC-Fe_3O_4 NPs resulted in a reduction of IL-6 levels at high exposure concentrations. The observed decrease in IL-6 levels is not due to absorbance of the cytokine onto the surface of the NP, as interference assays demonstrated no such effect (Guadagnini et al. 2015). Instead, this result is consistent with cytotoxicity and cell viability findings, whereby exposure to 75 µg/cm^2 OC-Fe_3O_4 caused trauma such that the majority of cells were killed. Similar effects on cell viability have also been seen following exposure of human brain-derived endothelial cells to U- and OC-coated Fe_3O_4 NPs (Halamoda Kenzaoui et al. 2012c). These results suggest different modes of action for Fe_3O_4 NP toxicity that is dependent upon the NP surface coating at higher exposure doses.

The surface charge was more negative for the OC-Fe_3O_4 NPs as compared with the U-Fe_3O_4 NPs. Studies of silver (Ag) NPs demonstrated that the more negatively charged NPs were less toxic against negatively charged Gram-positive bacteria (El Badawy et al. 2011). In a study of functionalised gold NPs it was determined that positively charged NPs were more cytotoxic than negatively charged NPs regardless of cell type to which they were exposed (Goodman et al. 2004). This is due to strong interactions with negatively charged membranes resulting in holes, membrane thinning or erosion (Leroueil et al. 2008, 2007). Therefore, one might expect that the less negatively charged U-Fe3O4 NPs would induce more cytotoxicity compared with OC-Fe_3O_4 NPs. However, there are factors other than charge to be taken into account.

The surface coating as well as surface charge of the Fe_3O_4 NPs will influence the protein corona formed around the NPs when exposed to cells in culture medium containing serum. This NP-protein coating composite determines the biological identity of the NP as perceived by the cell and hence the biological interaction and toxicity. Oxide NPs such as Fe_3O_4 have been shown to adsorb proteins onto their surface (Casals et al. 2011)

but the corona is dynamic over time as less motile proteins with greater surface affinity gradually replace more mobile proteins with lower affinity that bind initially. The formation of a ''hard corona'' takes place over days as opposed to hours. This may explain the altered toxicity response seen over time at the highest exposure for the U- and OC-Fe_3O_4 NPs. However, the most important driver in this system is likely to be the rapid formation of large agglomerates of U-Fe_3O_4 NPs. This extensively reduces the availability of individual U-Fe_3O_4 NPs in terms of surface area for internalisation by the BeWo b30 cells and hence the actual cellular exposure dose compared with OC-Fe_3O_4 NPs.

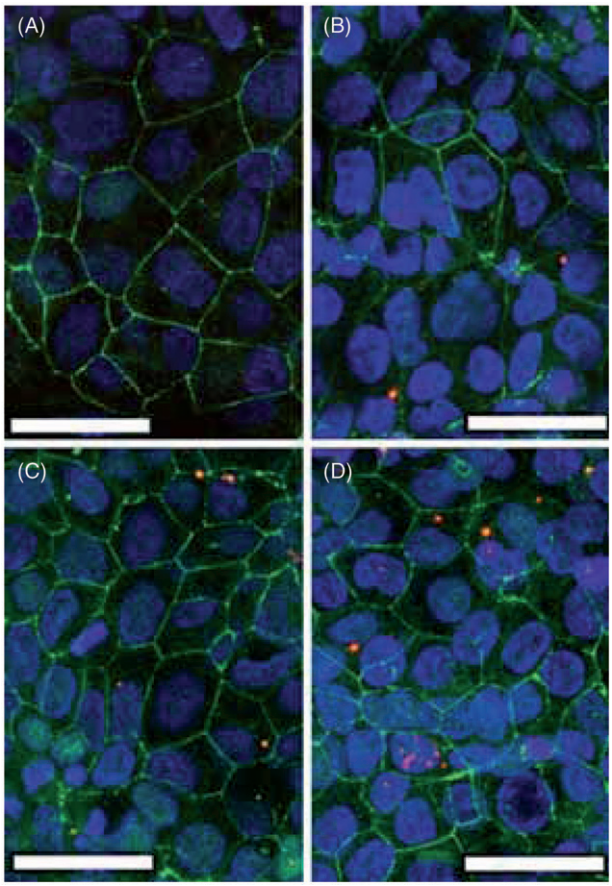

Figure 8. Confocal imaging of BeWo b30 cells after exposure to Fl-SiO_2 NPs. BeWo b30 cells were grown on PE membranes with 3 μm pore size after exposure to 25 nm (A and B) or 50 nm (C and D) Fl-SiO_2 NPs for 6 h. Exposure concentrations were 25 μg/ml (A and C) or 50 μg/ml (B and D). The scale bars represent 48 μm and Fl-SiO_2 NPs can be seen as red patches. Cell nuclei were stained with DAPI (blue), tight junctions with ZO-1 (green).

The dissolution of Fe_3O_4 NPs was not investigated in this study but it is likely that once internalised by the cell, degradation of the NPs into Fe ions within the lysosomes will occur, potentially giving rise to oxidative stress responses (Singh et al. 2010). This mechanism cannot be ruled out and requires further study in the BeWo b30 model looking at a comparison with maghemite (Fe_2O_3) and evaluation of the effect of adding an iron chelator.

IL-6 may play a role in maintaining the placenta during pregnancy, influencing barrier development and determining foetal development (Hsiao & Patterson 2012; Jiang et al. 2010; Robertson et al. 1994). Our results demonstrate that NPs can alter IL-6 release, albeit at high concentrations, so it is important to determine the effect of NPs upon this key cytokine, and more detailed studies are required.

The effect of Fl-SiO_2 particle size on toxicity was less pronounced compared to the differences seen in Fe_3O_4 NPs with different surface chemistry. In our studies with 25 and 50 nm Fl-SiO_2 NPs, very few differences were observed in terms of the toxicity pattern. However, the smaller-sized Fl-SiO_2 NPs tended to reduce cell viability but not membrane integrity at a lower exposure dose compared to the 50-nm-sized particles. While the size of Fl-SiO_2 NPs does not appear to influence disruption of cell membrane integrity, it may play a more significant role internally by influencing metabolic activity through endocytosis and disruption of the electron transport chain (Costa et al. 2010; Teodoro et al. 2011). Size and surface charge also play a role in determining the endocytic route (Hirn et al. 2011). Since our SiO_2 NPs had a similar surface charge (Table I), size may determine NP internalisation. An optimal size of 45–50 nm for efficient cellular uptake has been shown by several groups for gold NPs (Chithrani & Chan 2007; Chithrani et al. 2006; Nam et al. 2012; Wang et al. 2010). Below 45 nm, uptake increases with NP size and uptake rate has been shown to be highest for 45–50-nm-sized NPs, whereas exocytosis is faster for smaller NPs (Nam et al. 2012). Thus, we might expect to see enhanced intracellular toxicity for the 50 nm Fl-SiO_2 NPs compared to the same dose of 25 nm Fl-SiO_2 NPs in our study. The reason that we do not see this as most likely due to the overlap in size distribution of the Fl-SiO_2 NPs (Table I), particularly when suspended in cell-culture medium containing serum.

Figure 9. Tight junction staining of BeWo b30 cells exposed to 50 μg/ml (A) and 100 μg/ml (B) U-Fe_3O_4, and 50 μg/ml (C) and 100 μg/ml (D) OC-Fe_3O_4. Tight junctions were stained with ZO-1 (green), nuclei stained with DAPI (blue).White scale bar represents 48 μm.

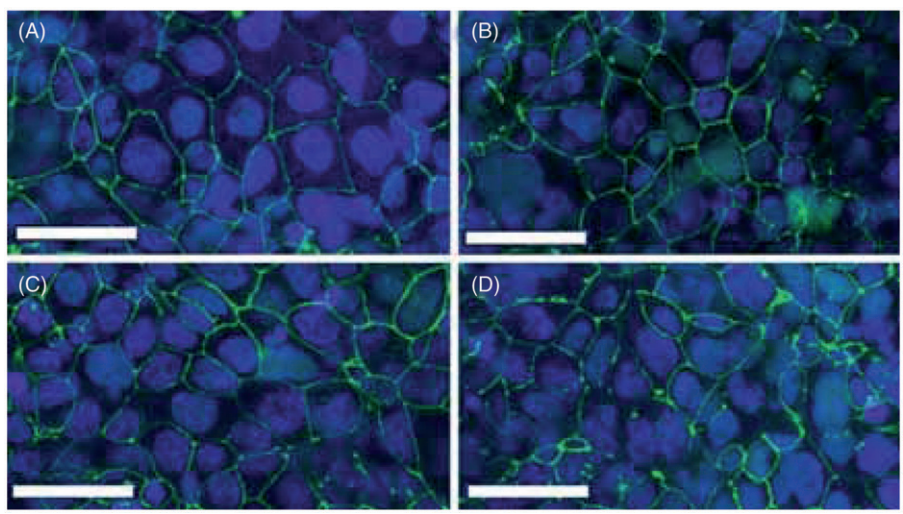

Using the BeWo b30 placenta cell barrier model, we have demonstrated that both OC-Fe_3O_4 and Fl-SiO_2 NPs are able to cross the cell barrier. The NP coating strongly influenced the transport with the OC-Fe_3O_4 NPs transferring across the barrier, whereas U-Fe_3O_4 NPs aggregated and precipitated onto the cell surface. Fl-SiO_2 NP transport across the cell barrier was unaffected by size which is not surprising given the overlap of size distribution mentioned above. The extent of transport of Fl-25 SiO_2 NP and Fl-50 SiO_2 NP across the barrier was very similar, as demonstrated by the comparable permeability coefficients and the percentage transport. Transport across the cell barrier was also unaffected by NP concentration. However, in the absence of cells, NP transport across the insert was proportional to NP concentration. Taken together, this indicates that the placental cells do act as a partial but not complete barrier to NP transport.

The high transport of NPs of ~24–29% was unexpected. No detectable transport of OC-Fe_3O_4 NPs across HCEC brain-derived endothelial cells or across intestinal barrier models was observed using NPs from the same source as our study (Halamoda Kenzaoui et al. 2012a, b). A recent study of Fl-SiO_2 NPs demonstrated low-level transport of 25 nm Fl-SiO_2 NPs in the BeWo b30 model with detectable levels that reached after 12 h (Poulsen et al. 2015). Whilst the NPs were from the same source in both studies there were differences in protocol and detection equipment, which could give rise to the different results.

Overestimation of transport data cannot be ruled out, mainly due to the NP detection methods used and inaccuracies in the measurements due to poor stability of NPs in cell-culture media. Furthermore, NP aggregation or agglomeration may occur in cell-culture media. Therefore, a 50 µl sample volume may not be representative for the entire sample chamber. Although every effort was made to mix the contents of the basal chamber before sampling, local agglomerates or aggregates of NPs may have been sampled, which could lead to an overestimate when extrapolating the data to the whole chamber volume. However, the consistency of the data indicates that there is NP transport across BeWo b30 cells and the more extensive transport compared with other barrier models such as blood–brain barrier and gut is in keeping with the greater permeability of the placenta. Careful consideration of the experimental set-up and the choice of detection method are particularly crucial when studying NPs in suspension as opposed to chemical liquids in solution to improve the quality of future results.

In terms of NP association with cells and potential cell uptake, we observed differences due to surface chemistry, namely surface charge. Fe_3O_4 NPs were taken up into the BeWo cells and it is likely that a clathrin-mediated endocytic pathway is involved in their transport across the cell membrane as shown for magnetic silica-coated NPs in A549 cells (Kim et al. 2006) and polystyrene NPs in MDCK-II cells (Fazlollahi et al. 2011). Most studies of NP endocytosis have focussed on non-polarised cells, so evaluation of the endocytic properties on the apical and basolateral sides of the BeWo b30 model in our future work will be important (Iversen et al. 2012). A study of polymeric NPs in the polarised MDCK system demonstrated that the surface charge of the NPs determined the endocytic and transcytotic path through the cell (Harush-Frenkel et al. 2008). Both cationic and anionic NPs exploited the clathrin endocytic pathway but there was also transcytosis and accumulation of NPs at the basolateral membrane and some anionic but not cationic NPs utilised the degradative lysosomal pathway. Coating the iron oxide particles with Na-oleate reduced their association with the cell layer, but TEM demonstrated that some OC-Fe_3O_4 NPs were internalised by the cells. Cell membranes possess a negative charge, and, therefore, the high negative surface charge of OC-Fe_3O_4 NP compared to U-Fe_3O_4 may be the reason for the observed difference in association with the cell membrane. Similarly, Fl-SiO_2 NPs, which are less strongly negatively charged than OC-Fe_3O_4, associated more with BeWo b30 cells compared to OC-Fe_3O_4 NP. An effect of size on association of Fl-SiO_2 was indicated but not clearly evident from the confocal images. Conclusions on cellular uptake of these NPs will require more detailed studies.

Extrapolation from this data to the transfer of NP *in vivo* is difficult since the placenta is a much more complex tissue. Limited placental transfer of 25 nm Fl-SiO2 NPs of ~4.2% after 6 h has been demonstrated in the perfused human placenta model (Poulsen et al. 2015). A study of 50–500 nm fluorescently labelled polystyrene NPs in the perfused placenta model resulted in the detection of NPs of up to 240 nm in the foetal circulation after 3-h perfusion (Wick et al. 2010). This argues against size as the restricting factor for placental transfer. Fluorescently tagged PAMAM dendrimers of around 6 nm transferred to the foetal circulation at low levels and could be located primarily in the intervillous spaces and outer rim of the villous branches (Menjoge et al. 2011) highlighting the complexity and large surface area of the placental circulation.

This study provides a firm basis for high-throughput evaluation of wide dose ranges prior to *in vivo* testing, which would be difficult to achieve with *ex vivo* perfusion. The medical dose of Fe_3O_4 NP used for MRI contrast imaging of the central nervous system corresponds to approximately 10 µg/cm^2 (Corot et al. 2004) suggesting that little placental toxicity might be expected from clinically relevant doses. However, the enhanced sensitivity of the foetus means that we cannot rule out direct effects that might arise from foetal exposure to lower doses.

Cell barriers are more complex *in vivo* incorporating basement membranes, stromal compartments and fine capillaries as well as active transport functions but the existing *in vitro* models are still valuable for preliminary screening as long as NPs are fully characterised and suitable detection methods are utilised.

Conclusions

This study demonstrates that transport and uptake of NPs occur *in vitro* in the BeWo b30 placental barrier model and that both toxic effects of NPs and their transport and association with cells are heavily dependent on the particles' surface chemistry. The effect of size on transport and toxicity was less pronounced in this study on 25 and 50 nm Fl-SiO_2 NPs perhaps reflecting the size overlap seen from NP characterisation. Further development of standardised model NPs to explore the characteristics driving toxicity and transport and of the placental barrier model is strongly recommended to allow more accurate extrapolation to *in vivo* exposure scenarios.

Acknowledgements

This study was supported by funding from the EU Framework 7 Health programme (contract 201335). The work by UH Bristol was carried out with the support of the Bristol Centre for Nanoscience and Quantum Information, University of Bristol. The authors thank Dr Mark Jepson, School of Biochemistry, University of Bristol, for his help with the confocal imaging, and Stuart Ferguson and John Schwieso, University of the West of England, for technical support.

Declaration of interest

The authors report no conflicts of interest. The authors alone are responsible for the content and writing of the paper.

References

Alexis F, Pridgen E, Molnar LK, Farokhzad OC. 2008. Factors affecting the clearance and biodistribution of polymeric nanoparticles. Mol Pharm 5(4):505–515.

Andreas K, Georgieva R, Ladwig M, Mueller S, Notter M, Sittinger M, et al. 2012. Highly efficient magnetic stem cell labeling with citrate-coated superparamagnetic iron oxide nanoparticles for MRI tracking. Biomaterials 33(18):4515–4525.

Brunner TJ, Wick P, Manser P, Spohn P, Robert N, Limbach LK, et al. 2006. In vitro cytotoxicity of oxide nanoparticles: comparison to asbestos, silica, and the effect of particle solubility. Environ Sci Technol 40(14):4374–4381.

Buerki-Thurnherr T, von Mandach U, Wick P. 2012. Knocking at the door of the unborn child: engineered nanoparticles at the human placental barrier. Swiss Med Weekly 142:w13559.

Cartwright L, Poulsen MS, Nielsen HM, Pojana G, Knudsen LE, Saunders M, et al. 2012. In vitro placental model optimization for nanoparticle transport studies. Int J Nanomedicine 7:497–510.

Casals E, Pfaller T, Duschl A, Oostingh GJ, Puntes VF. 2011. Hardening of the nanoparticle–protein corona in metal (Au, Ag) and oxide (Fe3O4, CoO, and CeO2) nanoparticles. Small 7(24):3479–3486.

Chithrani BD, Chan WC. 2007. Elucidating the mechanism of cellular uptake and removal of protein-coated gold nanoparticles of different sizes and shapes. Nano Lett 7(6):1542–1550.

Chithrani BD, Ghazani AA, Chan WC. 2006. Determining the size and shape dependence of gold nanoparticle uptake into mammalian cells. Nano Lett 6(4):662–668.

Choi J, Burns AA, Williams RM, Zhou Z, Flesken-Nikitin A, Zipfel WR, et al. 2007. Core-shell silica nanoparticles as fluorescent labels for nanomedicine. J Biomed Opt 12(6):064007–064011.

Choi KY, Liu G, Lee S, Chen X. 2012. Theranostic nanoplatforms for simultaneous cancer imaging and therapy: current approaches and future perspectives. Nanoscale 4(2):330–342.

Chu M, Wu Q, Yang H, Yuan R, Hou S, Yang Y, et al. 2010. Transfer of quantum dots from pregnant mice to pups across the placental barrier. Small 6(5):670–678.

Corot C, Petry KG, Trivedi R, Saleh A, Jonkmanns C, Le Bas J-F, et al. 2004. Macrophage imaging in central nervous system and in carotid atherosclerotic plaque using ultrasmall superparamagnetic iron oxide in magnetic resonance imaging. Invest Radiol 39(10):619–625.

Costa CS, Ronconi JVV, Daufenbach JF, Gonçalves CL, Rezin GT, Streck EL, et al. 2010. In vitro effects of silver nanoparticles on the mitochondrial respiratory chain. Mol Cell Biochem 342(1-2):51–56.

Dusinska M, Fjellsbø L, Magdolenova Z, Rinna A, Runden PE, Bartonova A, et al. 2009. Testing strategies for the safety of nanoparticles used in medical applications. Nanomedicine (London, England) 4(6):605.

El Badawy AM, Silva RG, Morris B, Scheckel KG, Suidan MT, Tolaymat TM. 2011. Surface charge-dependent toxicity of silver nanoparticles. Environ Sci Technol 45(1):283–287.

Ema M, Kobayashi N, Naya M, Hanai S, Nakanishi J. 2010. Reproductive and developmental toxicity studies of manufactured nanomaterials. Reprod Toxicol 30(3):343–352.

Fadeel B, Garcia-Bennett AE. 2010. Better safe than sorry: understanding the toxicological properties of inorganic nanoparticles manufactured for biomedical applications. Adv Drug Deliv Rev 62(3):362–374.

Fazlollahi F, Angelow S, Yacobi NR, Marchelletta R, Yu AS, Hamm-Alvarez SF, et al. 2011. Polystyrene nanoparticle trafficking across MDCK-II. Nanomedicine 7(5):588–594.

Gambarota G, van Laarhoven HW, Philippens M, Peeters WJ, Rijken P, van der Kogel A, et al. 2010. Assessment of blood hemodynamics by USPIO-induced R 1 changes in MRI of murine colon carcinoma. Appl Magn Reson 38(3):349–360.

Gao J, Hugger ED, Beck-Westermeyer MS, Borchardt RT. 2000. Estimating intestinal mucosal permeation of compounds using Caco-2 cell monolayers. In: Enna SJ, Williams M, Ferkany JW, Kenakin T, Porsolt RE, Sullivan JP, editors. Current protocols in pharmacology. New York: John Wiley & Sons, Unit 7.2. pp 1–23.

Goodman CM, McCusker CD, Yilmaz T, Rotello VM. 2004. Toxicity of gold nanoparticles functionalized with cationic and anionic side chains. Bioconjug Chem 15(4):897–900.

Guadagnini R, Halamoda B, Cartwright L, Pojana G, Magdolenova Z, Bilanicova D, et al. 2015. Toxicity screenings of nanomaterials: challenges due to interference with assay processes and components of classic in vitro tests. Nanotoxicology 9(S1):13–24.

Halamoda Kenzaoui B, Bernasconi CC, Hofmann H, Juillerat-Jeanneret L. 2012b. Evaluation of uptake and transport of ultrasmall superparamagnetic iron oxide nanoparticles by human brain-derived endothelial cells. Nanomedicine 7(1):39–53.

Halamoda Kenzaoui B, Chapuis Bernasconi C, Guney-Ayra S, Juillerat-Jeanneret L. 2012c. Induction of oxidative stress, lysosome activation and autophagy by nanoparticles in human brain-derived endothelial cells. Biochem J 441(3):813–821.

Halamoda Kenzaoui B, Vilà MR, Miquel JM, Cengelli F, Juillerat-Jeanneret L. 2012a. Evaluation of uptake and transport of cationic and anionic ultrasmall iron oxide nanoparticles by human colon cells. Int J Nanomedicine 7:1275–1286.

Harush-Frenkel O, Rozentur E, Benita S, Altschuler Y. 2008. Surface charge of nanoparticles determines their endocytic and transcytotic pathway in polarized MDCK cells. Biomacromolecules 9(2):435–443.

Hirn S, Semmler-Behnke M, Schleh C, Wenk A, Lipka J, Schäffler M, et al. 2011. Particle size-dependent and surface charge-dependent biodistribution of gold nanoparticles after intravenous administration. Eur J Pharm Biopharm 77(3):407–416.

Hsiao EY, Patterson PH. 2012. Placental regulation of maternal-fetal interactions and brain development. Dev Neurobiol 72(10):1317–1326.

Iversen NK, Frische S, Thomsen K, Laustsen C, Pedersen M, Hansen PB, et al. 2012. Superparamagnetic iron oxide polyacrylic acid coated γ-Fe2O3 nanoparticles do not affect kidney function but cause acute effect on the cardiovascular function in healthy mice. Toxicol Appl Pharmacol 266(2):276–288.

Jiang YJ, Lu B, Crumrine D, Elias PM, Feingold KR. 2010. IL-6 stimulates but is not essential for stratum corneum formation and permeability barrier development during gestation. Exp Dermatol 19(8):e31–e36.

Johnston H, Pojana G, Zuin S, Jacobsen NR, Møller P, Loft S, et al. 2013. Engineered nanomaterial risk. Lessons learnt from completed nanotoxicology studies: potential solutions to current and future challenges. Crit Rev Toxicol 43(1):1–20.

Johnston HJ, Hutchison G, Christensen FM, Peters S, Hankin S, Stone V. 2010. A review of the in vivo and in vitro toxicity of silver and gold particulates: particle attributes and biological mechanisms responsible for the observed toxicity. Crit Rev Toxicol 40(4):328–346.

Jones HN, Ashworth CJ, Page KR, McArdle HJ. 2006. Cortisol stimulates system A amino acid transport and SNAT2 expression in a human placental cell line (BeWo). Am J Physiol Endocrinol Metab 291(3): E596–E603.

Kim J-S, Yoon T-J, Yu K-N, Noh MS, Woo M, Kim B-G, et al. 2006. Cellular uptake of magnetic nanoparticle is mediated through energy-dependent endocytosis in A549 cells. J Vet Sci 7(4):321–326.

King BF. 1992. Comparative studies of structure and function in mammalian placentas with special reference to maternal-fetal transfer of iron. Am Zool 32:331–342.

Kumagai M, Sarma TK, Cabral H, Kaida S, Sekino M, Herlambang N, et al. 2010. Enhanced in vivo magnetic resonance imaging of tumors by PEGylated iron-oxide–gold core–shell nanoparticles with prolonged blood circulation properties. Macromol Rapid Commun 31(17): 1521–1528.

Lahtinen U, Honsho M, Parton RG, Simons K, Verkade P. 2003. Involvement of caveolin-2 in caveolar biogenesis in MDCK cells. FEBS Lett 538(1-3):85–88.

Leroueil PR, Berry SA, Duthie K, Han G, Rotello VM, McNerny DQ, et al. 2008. Wide varieties of cationic nanoparticles induce defects in supported lipid bilayers. Nano Lett 8(2):420–424.

Leroueil PR, Hong S, Mecke A, Baker Jr JR, Orr BG, Banaszak Holl MM. 2007. Nanoparticle interaction with biological membranes: does nanotechnology present a Janus face? Acc Chem Res 40(5):335–342.

Liu F, Soares MJ, Audus KL. 1997. Permeability properties of monolayers of the human trophoblast cell line BeWo. Am J Physiol 273(5):C1596–C1604.

Mahmoudi M, Serpooshan V, Laurent S. 2011. Engineered nanoparticles for biomolecular imaging. Nanoscale 3(8):3007–3026.

Medina C, Santos-Martinez MJ, Radomski A, Corrigan OI, Radomski MW. 2007. Nanoparticles: pharmacological and toxicological significance. Br J Pharmacol 150(5):552–558.

Menjoge AR, Rinderknecht AL, Navath RS, Faridnia M, Kim CJ, Romero R, et al. 2011. Transfer of PAMAM dendrimers across human placenta: Prospects of its use as drug carrier during pregnancy. J Control Release 150(3):326–338.

MHRA. 2007. Device bulletin. Safety guidelines for Magnetic Resonance Imaging equipment in clinical use. Department of Health. http://www.mhra.gov.uk/home/groups/dts-iac/documents/publication/con2033065.pdf.Accessed on 27 March 2013.

Myllynen PK, Loughran MJ, Howard CV, Sormunen R, Walsh AA, Vähäkangas KH. 2008. Kinetics of gold nanoparticles in the human placenta. Reprod Toxicol 26(2):130–137.

Nam J, Won N, Bang J, Jin H, Park J, Jung S, et al. 2012. Surface engineering of inorganic nanoparticles for imaging and therapy. Adv Drug Deliv Rev 65(5):622–648.

Naqvi S, Samim M, Abdin M, Ahmed FJ, Maitra A, Prashant C, et al. 2010. Concentration-dependent toxicity of iron oxide nanoparticles mediated by increased oxidative stress. Int J Nanomedicine 5:983–989.

Nyström AM, Fadeel B. 2012. Safety assessment of nanomaterials: implications for nanomedicine. J Control Release 161(2):403–408.

Poulsen MS, Mose T, Maroun LL, Mathiesen L, Knudsen LE, Rytting E. 2015. Kinetics of silica nanoparticles in the human placenta. Nanotoxicology 9(S1):79–86.

Qiao R, Yang C, Gao M. 2009. Superparamagnetic iron oxide nanoparticles: from preparations to in vivo MRI applications. J Mater Chem 19(35):6274–6293.

Robertson SA, Seamark RF, Guilbert LJ, Wegmann TG. 1994. The role of cytokines in gestation. Crit Rev Immunol 14(3-4):239–292.

Rosen JE, Chan L, Shieh DB, Gu FX. 2012. Iron oxide nanoparticles for targeted cancer imaging and diagnostics. Nanomedicine 8(3):275–290.

Rümenapp C, Gleich B, Haase A. 2012. Magnetic nanoparticles in magnetic resonance imaging and diagnostics. Pharm Res 29:1165–1179.

Sadauskas E, Wallin H, Stoltenberg M, Vogel U, Doering P, Larsen A, et al. 2007. Kupffer cells are central in the removal of nanoparticles from the organism. Part Fibre Toxicol 4:10.

Saunders M. 2009. Transplacental transport of nanomaterials. Wiley Interdiscip Rev Nanomed Nanobiotechnol 1(6):671–684.

Sekhon BS, Kamboj SR. 2010. Inorganic nanomedicine—part 1. Nanomedicine 6(4):516–522.

Semmler-Behnke M, Kreyling WG, Lipka J, Fertsch S, Wenk A, Takenaka S, et al. 2008. Biodistribution of 1.4- and 18-nm gold particles in rats. Small 4(12):2108–2111.

Singh N, Jenkins GJ, Asadi R, Doak SH. 2010. Potential toxicity of superparamagnetic iron oxide nanoparticles (SPION). Nano Rev 1:doi: 10.3402/nano.v3401i3400.5358.

Sumner SC, Fennell TR, Snyder RW, Taylor GF, Lewin AH. 2010. Distribution of carbon-14 labeled C60 ([14C]C60) in the pregnant and in the lactating dam and the effect of C60 exposure on the biochemical profile of urine. J Appl Toxicol 30(4):354–360.

Tang F, Li L, Chen D. 2012. Mesoporous silica nanoparticles: synthesis, biocompatibility and drug delivery. Adv Mater 24(12):1504–1534.

Tang J, Xiong L, Wang S, Wang J, Liu L, Li J, et al. 2009. Distribution, translocation and accumulation of silver nanoparticles in rats. J Nanosci Nanotechnol 9(8):4924.

Teodoro JS, Simões AM, Duarte FV, Rolo AP, Murdoch RC, Hussain SM, et al. 2011. Assessment of the toxicity of silver nanoparticles in vitro: a mitochondrial perspective. Toxicol In Vitro 25(3):664–670.

Unfried K, Albrecht C, Klotz L-O, Von Mikecz A, Grether-Beck S, Schins RP. 2007. Cellular responses to nanoparticles: Target structures and mechanisms. Nanotoxicology 1(1):52–71.

Wahajuddin SA. 2012. Superparamagnetic iron oxide nanoparticles: magnetic nanoplatforms as drug carriers. Int J Nanomedicine 7: 3445–3471.

Wang S-H, Lee C-W, Chiou A, Wei P-K. 2010. Size-dependent endocytosis of gold nanoparticles studied by three-dimensional mapping of plasmonic scattering images. J Nanobiotechnology 8(1):33.

Wick P, Malek A, Manser P, Meili D, Maeder-Althaus X, Diener L, et al. 2010. Barrier capacity of human placenta for nanosized materials. Environ Health Perspect 118(3):432.

Yamashita K, Yoshioka Y, Higashisaka K, Mimura K, Morishita Y, Nozaki M, et al. 2011. Silica and titanium dioxide nanoparticles cause pregnancy complications in mice. Nat Nanotechnol 6(5):321–328.

Yang F, Jin C, Subedi S, Lee CL, Wang Q, Jiang Y, et al. 2012. Emerging inorganic nanomaterials for pancreatic cancer diagnosis and treatment. Cancer Treat Rev 38(6):566–579.

Yigit MV, Moore A, Medarova Z. 2012. Magnetic nanoparticles for cancer diagnosis and therapy. Pharm Res 29:1180–1188.

Zhang L, He R, Gu H-C. 2006. Oleic acid coating on the monodisperse magnetite nanoparticles. Appl Surface Sci 253(5):2611–2617.

Zhao W, Wang L, Tan W. 2007. Fluorescent nanoparticle for bacteria and DNA detection. Bio-Applications of Nanoparticles: Springer. Adv Exp Med Biol 620:129–135.

Zhong W. 2009. Nanomaterials in fluorescence-based biosensing. Anal Bioanal Chem 394(1):47–59.

Zou P, Yu Y, Wang YA, Zhong Y, Welton A, Galbán C, et al. 2010. Superparamagnetic iron oxide ''nanotheranostics'' for targeted cancer cell imaging and pH-dependent intracellular drug release. Mol Pharm 7(6):1974.